Published July 7, 2016

Journal of Environmental Quality

TECHNICAL REPORTS

SURFACE WATER QUALITY

Assessing the Influence of Calcium Fluoride on Pyrite Electrochemical Dissolution and Mine Drainage pH

Luying Wang, Qingyou Liu, Kai Zheng, and Heping Li*

Abstract

We investigated the influence of dissolved calcium fluoride, CaF_2(aq), on the electrochemical dissolution of pyrite and the corresponding environmental effects on acid mine drainage (AMD). The experimental results showed that CaF_2(aq) promotes pyrite electrochemical dissolution. When the CaF_2(aq) concentration increased from 0 to 10 mg L^{-1} up to saturation, the promoting efficiency was 15.80 and 57.25%, respectively. The reason for this phenomenon is that F^- and Fe^{2+} form FeF_2, and at a higher scan potential, F^- and Fe^{3+} form the ion complex FeF_6^{3-}. The mechanisms include: (i) the decreasing charge transfer resistance at the double layer due to the iron fluorine complex formation; and (ii) the decreasing passivation resistance at the cover layer due to the strong penetration of F^- ions through it into the double layer. Although the hydrolysis reaction of F^- in solution could increase the pH value of mine drainage, the AMD was significantly aggravated because CaF_2(aq) promoted the pyrite electrochemical dissolution.

Core Ideas

- Results showed CaF_2 could effectively promote pyrite electrochemical dissolution.
- F^- and Fe^{2+} form FeF_2, and at a higher scan potential, F^- and Fe^{3+} form the complex FeF_6^{3-}.
- Iron fluorine complex formation decreases charge transfer resistance at the double layer.
- Strong penetration of F^-into the double layer decreases the resistance at the cover layer.
- AMD was significantly aggravated because CaF_2 promoted the pyrite dissolution.

Pyrite is one of the most abundant sulfide minerals in the Earth's crust (Peters and Majima, 1968), and it is associated with coal and metal ore deposits. The oxidation of pyrite can form extremely acidic drainages (as low as pH 2). These acidic drainages are enriched with Fe, Mn, Al, SO_4, and occasionally heavy metals, such as Pb, Hg, Cd or As, and can contaminate streams, rivers and lakes, threatening the biota and the ecological balance (Evangelou and Zhang, 1995). Therefore, studies on pyrite oxidation and its environmental impacts have continuously increased in recent decades. The electrochemical characteristics and oxidation mechanisms of pyrite under biotic (e.g., *Acidithiobacillus thiooxidans* and *Acidithiobacillus ferrooxidans*) and abiotic conditions have been widely investigated using different techniques, including potentiodynamic polarization measurements (Yang and Jiang, 1991; Giannetti et al., 2006), cyclic voltammetry (Palencia et al., 1991; Giannetti et al., 2001; Constantin et al., 2014), electrochemical impedance spectroscopy (EIS) (Cabral and Ignatiadis, 2001; Lehner et al., 2008), steady state photocurrent (Chen et al., 1991; Constantin and Chirita, 2013), and surface techniques, such as scanning photoelectron microscopy (Chandra and Gerson, 2011), X-ray photoelectron spectroscopy (Giannetti et al., 2001; Bryson and Crundwell, 2014), grazing incidence X-ray diffraction (Marco et al., 2006), Fourier transform infrared spectroscopy (Kelsall et al., 1999; Chernyshova, 2004), and Rutherford backscattering spectrometry (Pratesi and Cipriani, 2000). The pyrite oxidation processes are complex, involve chemical, biological, and electrochemical reactions, and vary with environmental conditions. There is no single-rate formula that describes the kinetics of pyrite oxidation for all cases (Evangelou and Zhang, 1995). Generally, the progress of acid mine drainage (AMD) can be described by the following equations (Singer and Stumm, 1970; Weber et al., 2004):

$$FeS_2 + \frac{7}{2}O_2 + H_2O \rightarrow Fe^{2+} + 2SO_4^{2-} + 2H^+ \quad [1]$$

$$Fe^{2+} + \frac{1}{4}O_2 + H^+ \rightarrow Fe^{3+} + \frac{1}{2}H_2O \quad [2]$$

J. Environ. Qual. 45:1344–1350 (2016)
doi:10.2134/jeq2015.06.0275
Received 11 June 2015.
Accepted 21 Dec. 2015.
*Corresponding author (liheping123@yahoo.com).

L. Wang, Q. Liu, K. Zheng, and H. Li, Key Laboratory of High-Temperature and High-Pressure Study of the Earth's Interior, Institute of Geochemistry, Chinese Academy of Sciences, Guiyang 550002, China; L. Wang and K. Zheng, Univ. of Chinese Academy of Sciences, Beijing, 100049, China. Assigned to Associate Editor Markus Grafe.

Abbreviations: AMD, acid mine drainage; CPE_p, constant phase element; E_{corr}, corrosion potential; EIS, electrochemical impedance spectroscopy; EEC, electrochemical equivalent circuit; i_{corr}, corrosion current density; OCP, open circuit potential; R_p, polarization resistance.

$$Fe^{3+} + 3H_2O \rightarrow Fe(OH)_3(s) + 3H^+ \quad [3]$$

$$FeS_2 + 7Fe_2(SO_4)_3 + 8H_2O \rightarrow 15FeSO_4 + 8H_2SO_4 \quad [4]$$

Geologists have investigated the oxidation of natural pyrite based on stable isotope geochemistry and geomicrobiology. In natural environments, the elucidation of pyrite oxidation energetics and kinetics requires integration of available hydrogeochemical, isotopic, and microbiological data (Taylor et al., 1984). To better understand the reaction pathways of pyrite oxidation, Balci et al. (2007) conducted a series of pyrite oxidation experiments that involved biogeochemically controlling the $\delta^{18}O$ and $\delta^{34}S$ values of the generated sulfate in AMD and in other natural environments. Their results suggested that Fe(III)(aq) was the primary oxidant of pyrite at pH < 3, and water was the primary oxygen source for sulfate.

Many studies have contributed to the creation of an inventory of AMD precipitates to better understand the sources of AMD distribution. Galán et al. (2003) studied the profiles of Fe, Mn, and potentially toxic trace elements (As, Cd, Cr, Cu, Ni, Pb, and Zn) in sediments historically contaminated with AMD and suggested that Fe oxy-hydroxides play a dominate role in the metal accumulation. Sarmiento et al. (2007) investigated arsenic speciation in AMD from the Iberian Pyrite Belt and suggested that As(III) was eliminated through adsorption onto Fe precipitates after being photooxidized to As(V). España et al. (2005) found that the characteristics of AMD solutions varied with hydro-geochemical, mineralogical and environmental factors. Many other studies have investigated AMD based on geochemistry and stable sulfur and oxygen isotopes (Migaszewski et al., 2008; Gammons et al., 2010).

The pH of AMD is a key factor in the prevention of mining pollution. The removal of heavy metals from AMD depends on the wastewater pH (Sheoran and Sheoran, 2006). Ferric iron is effectively removed at a pH up to 3.5 with sufficient retention for subsequent precipitation of iron hydroxides (Mueller et al., 2003). Aluminum is precipitated as aluminum hydroxides at pH 5 (Hedin et al., 1994). Manganese can only be removed when the pH is close to 8 (Stumm and Morgan, 1981). The absorption capacity of heavy metals onto sediments or soils is dramatically weakened in acidic environments (Wang et al., 2012). Therefore, the acidity of AMD resulting from pyrite electrochemical dissolution is concerning.

Fluorite and pyrite are often found in fluorite–quartz–pyrite and sulfide mineralization (Ixer et al., 1996; Zhai et al., 2014). Fluoride ions enter groundwater through the weathering of rocks that are rich in fluoride. CaF_2 originating from igneous and sedimentary rocks (Chang et al., 1998) has caused health problems in people from more than 25 nations (Brindha and Elango, 2011). During mining production, fluoride ions can inhibit bacterial growth and iron bio-oxidation that affects the biohydrometallurgical processes of minerals (Veloso et al., 2012). Therefore, research on the effects of fluorite on pyrite electrochemical dissolution is required.

To date, few quantitative data have been reported on the influence of F^- on the electrochemical dissolution of pyrite. In this study, we used polarization curves and environmental impedance spectroscopy (EIS) to investigate the electrochemical dissolution of pyrite in a sulfuric acid solution with varying concentrations of calcium fluoride to reveal the oxidation mechanism of pyrite under the influence of F^-. In addition, the dynamic changes in the solution pH of pyrite pulp were measured under varying concentrations of calcium fluoride to understand the effect of calcium fluoride on AMD.

Materials and Methods

Electrode Preparation

Pyrite samples were purchased from Ward's Natural Science. Inductively coupled plasma optical emission spectrometry (Varian Vista-Pro ICP-OES) was used for elemental analysis of the pyrite samples. The impurity level present in the sample was less than 4.0% g g^{-1} (Table 1). The pyrite electrode was prepared by cutting the pyrite sample into approximately a cubic shape with working areas of 0.30 cm^2, and these cubic samples had no visible imperfections. After cleaning them in detergent, ethanol, and ultrapure water, the specimens were placed on an epoxy resin, and each was connected to a copper wire using silver paint on its back face, leaving only one face of the electrode exposed to the solution. Before each test, the mineral electrode was polished with carbide paper (1200 grit count) to obtain a fresh surface, degreased using alcohol, rinsed with deionized water and dried in a stream of air.

Electrochemical Measurements

Electrochemical measurements were performed using a computer-controlled electrochemical measurement system (PARSTAT 2273, Princeton Applied Research) with a conventional three-electrode electrolytic cell that included a platinum auxiliary electrode, a pyrite working electrode, and a saturated calomel reference electrode. All other potentials in this study are quoted relative to the saturated calomel reference electrode (0.242 V vs. standard hydrogen electrode), unless otherwise stated. To minimize the resistance of solution between the working electrode and the reference electrode, the reference electrode was connected to a Luggin capillary.

The electrolyte was adjusted to pH 2.0 with H_2SO_4, and four treatments of calcium fluoride were added: 0, 10.0, 50.0 mg L^{-1}, and saturation. We calculated that the saturated concentration of calcium fluoride in a pH 2 solution was approximately 96.9 mg L^{-1}, as the equilibrium constants of HF and CaF_2 are 6.76×10^{-4} (Ryzhenko, 1965) and $3.08 \pm 0.08 \times 10^{-11}$ (Garand and Mucci, 2004), respectively. When the electrolyte contained CaF_2, CaF_2 is dissolved and the ions exist as Ca^{2+} and F^-, which is stated as CaF_2(aq). Electrolyte (25 mL) was used in each test. The working, auxiliary, and reference electrodes were situated in the same location to ensure a uniform spatial relationship. The experiments were conducted at 25 ± 1°C by a water bath.

Polarization curves were obtained by changing the electrode potential automatically from −250 to +250 mV (vs. open

Table 1. Chemical composition of the pyrite sample.

	Cu	Fe	S	Ca	Zn	Pb	SiO_2
% g g^{-1}	0.18	45.0	51.0	0.05	0.20	0.47	3.10

circuit potential, OCP) at a scan rate of 10 mV s^{-1}. The corrosion potential (E_{corr}), the corrosion current density (i_{corr}), and the Tafel slopes of the anode (b_a) and cathode (b_c) were derived from the polarization curves based on the extrapolation methods (Bard and Faulkner, 2001). Furthermore, the polarization resistance values, R_p, were calculated from the Stern–Geary equation (Stern and Geary, 1957) in which

$$R_p = \frac{b_a b_c}{2.3 \times i_{corr} \times (b_a + b_c)} \quad [5]$$

In this study, η is defined as

$$\eta = \frac{i_{corr} - i^0_{corr}}{i^0_{corr}} \times 100 \quad [6]$$

which is used as the inhibition efficiency in materials science (Solmaz et al., 2008; Wang et al., 2011). The EIS tests were performed at the OCP and over a frequency range of 0.001 to 10,000 Hz and amplitude of 10 mV, and ZSimpWin 3.20 software (Yeum, 2004) was then used to fit the impedance data. To ensure reproducibility, identical experiments were repeated at least three times to ensure that the reported results were reproducible (i.e., the random errors of all three identical experimental results were within tolerance), and all of the reported results in this study were averaged.

Before the polarization curves and EIS tests, the OCP tests were performed. During the OCP test, the electrode potential increased for 5 min and then reached a quasi-steady state, defined here as a change of less than 2 mV per 5 min. Then, the electrode was stabilized for 400 s, and the potential was recorded as the OCP. During the second and third identical experiments, if the potential at the quasi-steady state was not within ±5 mV of the first test, then the OCP test was terminated, and a new test was performed until the same OCP as the first test was obtained when stabilized for approximately 400 s.

Effect of Calcium Fluoride on Pyrite Pulp pH

Three Erlenmeyer flasks filled with 200 mL of deionized water were used for these experiments. The acidity of the deionized water was adjusted to pH 4.0 using H_2SO_4 to prompt calcium fluoride dissolution to obtain a 10 mg L^{-1} calcium fluoride solution and to prompt pyrite corrosion by the acidic solution through the following steps. Different quantities (0, 2, and 10 mg) of calcium fluoride were added to the flasks to yield the 0, 10 mg L^{-1} and saturated calcium fluoride solutions, respectively. We calculated that the saturated concentration of CaF_2(aq) in a pH 4 solution was approximately 16.7 mg L^{-1}. Finally, two grams of pyrite (<74 μm diam.) was added to each solution. The pulp pH was measured after 1, 2, 3, 5, 8, 13, 15, 18, 21, 24, 27, 29, 34, 38, 42, 44, 47, 50, 54, 58, and 60 d, respectively. All experiments were conducted at 25 ± 1°C by a water bath.

Results and Discussion

Polarization Curves

Polarization curves investigate the electrochemical corrosion rate and electrochemical corrosion susceptibility by measuring the corresponding current densities in different electrode potentials. In the present study, we used polarization curves as the fundamental method for corrosion analysis and phenomenon elucidation of the electrode (Tachibana et al., 2009).

By increasing the CaF_2(aq) concentration from 0 to 10 mg L^{-1}, the i_{corr} of the pyrite electrode increased from 0.386 to 0.447 μA cm^{-2}, and the E_{corr} increased from 234.1 to 239.7 mV. These values further increased to 0.607 μA cm^{-2} and 244.6 mV, respectively, when CaF_2(aq) reached saturation (Fig. 1, Table 2). Constantin and Chirita (2013), Ouyang et al. (2015) and Wang et al. (2010) reported corrosion current values of 1.78, 1.801, and 0.876 μA cm^{-2}, respectively, under similar experimental conditions. The i_{corr} value which used electrolytes lacking CaF_2(aq) in the present study (0.386 μA cm^{-2}) was smaller than in the abovementioned studies due to different concentrations of H^+, the chemical compositions of the mineral samples, the amounts of available oxygen in solution, and the scan rates (Table 3).

When the electrolyte contained CaF_2(aq), CaF_2(aq) promoted the pyrite electrochemical interaction. The promoting efficiency (η) was 15.80% when the CaF_2(aq) concentration increased from 0 to 10 mg L^{-1}, and it increased to 57.25% when CaF_2(aq) increased from 0 mg L^{-1} to saturation. CaF_2(aq) promotes pyrite electrochemical interaction by decreasing the pyrite polarization resistance R_p. Specifically, R_p decreased from 91.9 to 78.7 Ω cm^2 with increasing concentrations of CaF_2(aq) from 0 to 10 mg L^{-1}, and it further decreased to 57.3 Ω cm^2 when CaF_2(aq) was saturated.

The Tafel slopes of the polarization curves with respect to anodes and cathodes in our study were obtained by the Tafel extrapolation method in the high-polarization area (~420–450 and ~100–120 mV, respectively; Lefebvre, 2002). This method provides information relevant to reaction mechanisms depending on the reaction conditions. In the anodic curves, the Tafel slopes of the anode (b_a) decreased at higher concentrations of CaF_2(aq) in the electrolyte, indicating that the anode processes were stimulated in the Tafel area. There are two probable causes for this phenomenon. First, the pyrite corrosion potential becomes more positive as the CaF_2(aq) concentration increases, and the higher corrosion potential could promote dissolution of the pyrite anode as shown in Reaction [7] (Lowson, 1982;

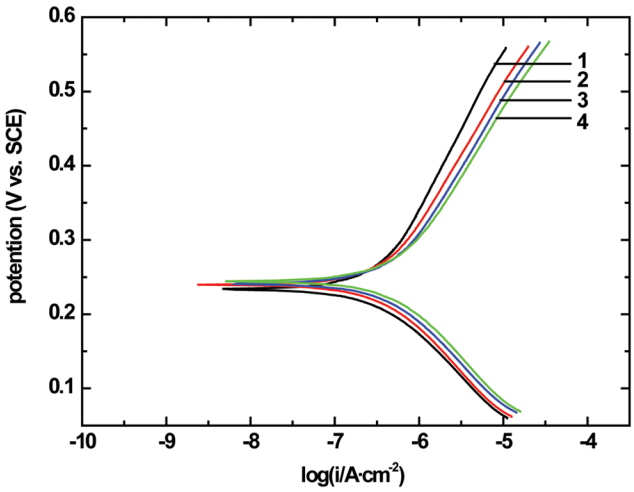

Fig. 1. Potentiodynamic curves of the pyrite electrode under different CaF_2(aq) concentrations: (1, black line) 0 mg L^{-1}, (2, red line) 10.0 mg L^{-1}, (3, blue line) 50.0 mg L^{-1}, and (4, green line) saturated.

Table 2. Electrochemical parameters† of FeS_2.

CaF_2 concentration	E_{corr}	b_a	b_c	i_{corr}	R_p	η‡
mg L^{-1}	mV			μA cm^{-2}	Ω cm^2	%
0	234.1	235.9	125.0	0.386	91.9	
10	239.7	203.6	134.3	0.447	78.7	15.80
50	241.2	199.6	135.8	0.541	65.0	40.16
saturated	244.6	192.2	137.1	0.607	57.3	57.25

† E_{corr}, corrosion potential; b_a, Tafel slope of the anode; b_c, Tafel slope of the cathode; i_{corr}, corrosion current density; R_p, polarization resistance.

‡ $\eta = (i_{corr} - i^0_{corr})/ i^0_{corr} \times 100$

Table 3. Experimental conditions of different authors.

Reference	Electrolyte	Scan rate	Chemical composition of pyrite
		mV s^{-1}	%Fe:%S
This work	25°C, ultrapure water, pH 2 (used H_2SO_4 to adjust)	10	45:51
Constantin and Chirita (2013)	25°C, distilled water with saturated oxygen, pH 2.5 (used HCl to adjust)	1	46.57:53.23
Ouyang et al. (2015)	25°C, 0.1 M Na_2SO_4, pH 2 (used H_2SO_4 to adjust)	1	46.46:53.1
Wang et al. (2010)	25°C, 0.1 M KNO_3, pH 2.5 (used KOH + HNO_3 to adjust)	0.15	45.09:54.91

Alloway and Ayres, 1997). However, the dominant cause involves the FeF_2 formation from F^- and Fe^{2+} as shown in Reaction [8]. It is worth to note that during the fast anodic scan process, Fe^{2+} ions produced and its local high concentration on pyrite electrode surface was enough for the formation of FeF_2 due to its sparingly solubility (25°C, solubility product constant is 2.36×10^{-6}, solubility is 0.4962 g 100 g^{-1} in pH 2 solution; Greenwood and Earnshaw, 1997). The formation of FeF_2 solids reduces the concentration of aqueous Fe^{2+} promoting pyrite dissolution. Obviously, FeF_2 was unstable, and it dissolved during the anodic scan process. As the anodic scan potential increased, ferrous ions would be further oxidized to ferric ions as shown in Reaction [9] (Stumm and Lee, 1961; Hiskey and Schlitt, 1982; Chander and Briceno, 1987). Fluoride and ferric ions would then form FeF_6^{3-} ion complexes ($K_f = 10^{15.04}$) as shown in Reaction [10] (Hocking et al., 2010), resulting in the decreasing Fe^{3+} concentration in the electrolyte, which further stimulated pyrite oxidation.

$$FeS_2 + 8H_2O \rightarrow Fe^{2+} + 2SO_4^{2-} + 16H^+ + 14e^- \quad [7]$$

$$Fe^{2+} + 2F^- \rightarrow FeF_2 \quad [8]$$

$$Fe^{2+} \rightarrow Fe^{3+} + e^- \quad [9]$$

$$Fe^{3+} + 6F^- \rightarrow FeF_6^{3-} \quad [10]$$

In contrast to the anode, the Tafel slopes of the cathode (b_c) increased with the increasing CaF_2(aq) concentration in the electrolyte, suggesting that the cathodic processes were inhibited. In this study, the cathodic reaction, Reaction [11], consisted of oxygen reduction. Therefore, the reason for this phenomenon is related to the amount of oxygen present in solution. Moslemi et al. (2011) reported that the presence of chloride and sulfate ions in solution reduced the amount of available oxygen in solution, and Geng and Duan (2010) provided a detailed theoretical explanation and mathematical derivation of the above oxygen solubility phenomenon, which revealed that the solubility of oxygen in brine system decreased with increasing salt concentration. When CaF_2 was added to the electrolyte, the presence of fluoride and calcium ions in solution reduced the amount of available oxygen in solution. Oxygen is a strong oxidant, and its decrease in concentration would consequently inhibit the cathodic reaction.

$$O_2 + 4H^+ + 4e^- \rightarrow 2H_2O \quad [11]$$

Electrochemical Impedance Spectroscopy

Electrochemical impedance spectroscopy (EIS) provides information on the mineral's interface structure and surface redox reactions by applying a periodic, low-amplitude, alternating current signal at different frequencies to the target. In the present study, we used EIS to study the characteristics of the electrodes and electrochemical reactions (Orazem and Tribollet, 2008).

The Nyquist plots were composed of a distorted capacitive loop (coming from two capacitive loops, Fig. 2). The first, obtained at high frequencies, is attributed to the charge transfer resistance (R_t) corresponding to the resistance between pyrite and the outer Helmholtz plane. The second, obtained at low frequencies, was slightly distorted, which is related to the combination of pseudo-capacitance impedance (due to the passive layer) and a resistance R_p. Deviation from an ideal semicircle is generally attributed to frequency dispersion and inhomogeneities in the passive layer surface. The related electrochemical equivalent circuit (EEC) used to model the pyrite/electrolyte interface is shown in Fig. 3. Constantin and Chirita (2013) and Ouyang et al. (2015) used this model to explain the oxidative dissolution of pyrite in acidic media, and Pang et al. (1990) provided a detailed theoretical explanation of this EEC model. Because the equivalent circuits represent an approach to describe the electrochemical processes that occur at the electrode and/or electrolyte interface, any model derived from them is only tentative (Macdonald, 1985). For this reason, different EECs were used to fit the EIS data, and only the results that best fit our proposed model are shown (Table 4).

As the CaF_2(aq) concentration increased, the C_{dl} value increased, while the R_t value decreased. The increasing C_{dl} values were attributed to the increases in the local dielectric constant due to the fluorinated complex formation and reduction at the electrode/solution interface. A higher C_{dl} and lower

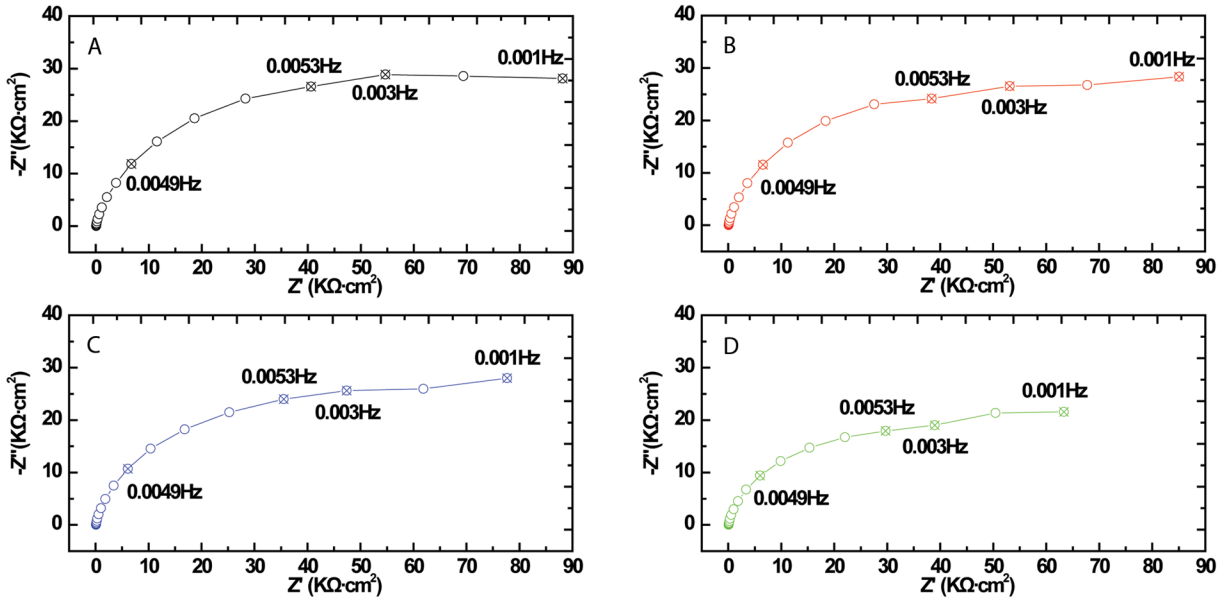

Fig. 2. Nyquist plots of the pyrite electrode at open circuit potential under different CaF_2(aq) concentrations: (A) 0 mg L^{-1}, (B) 10.0 mg L^{-1}, (C) 50.0 mg L^{-1}, and (D) saturated. Z′/Z″ denotes the real/imaginary parts of the impedance, respectively.

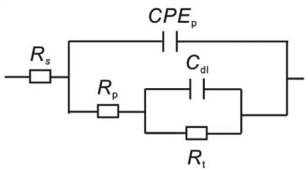

Fig. 3. Equivalent circuit for the pyrite electrode/electrolyte at open circuit potential. R_s indicates electrolyte and other ohmic resistance, R_t indicates charge transfer resistance, R_p indicates film resistance, C_{dl} indicates double layer capacitance, CPE_p represents constant phase element.

R_t indicate that charges diffuse more easily through the electric double layers, that is, the electrochemical dissolution of the pyrite electrode required less energy. These results are in agreement with those from the polarization study. In addition, the capacitance parameter (CPE_p) increased, and the film resistance R_p decreased as the concentration of CaF_2(aq) increased. The value of CPE_p characterizes the extent of ions that could diffuse through and accumulate on the passive film, and the R_p value reveals the extent of the passive film that could inhibit mineral dissolution. Larger CPE_p and lower R_p values indicate that the passive film had a lower capability to inhibit mineral dissolution because F^- ions could penetrate the passive film due to their small ionic radius. The smaller exponent n values suggest that the degree of passive film inhomogeneity increased with increasing CaF_2(aq) concentration.

Effect of Calcium Fluoride on Pyrite Pulp pH

During the first 3 d, pyrite pulp without added CaF_2 decreased slightly in pH (Fig. 4). This phenomenon reflects the electrochemical dissolution of pyrite, $FeS_2 + 7/2O_2 + H_2O \rightarrow Fe^{2+} + 2SO_4^{2-} + 2H^+$ (Reaction [1]), which includes two half-reactions, the anodic reaction $FeS_2 + 8H_2O \rightarrow Fe^{2+} + 2SO_4^{2-} + 16H^+ + 14e^-$ (Reaction [7]) and the cathodic reaction $O_2 + 4H^+ + 4e^- = 2H_2O$ (Reaction [11]). The anodic oxidation products were sulfate and sulfite ions and sulfur; however, a common view is that sulfur, or iron-deficient sulfur-rich surfaces, or sulfite act as an intermediate, and the terminal products are only sulfate ions (McKay, 1957; Hall et al., 1985; Luther, 1987). When electrolyte contained CaF_2(aq), F^- ions promoted pyrite electrochemical interaction and resulted in more H^+. But on the other hand, F^- can hydrolyze in solution, that is, $F^- + H_2O = HF + OH^-$, leading to a pH greater than 4 (pH initial value). That is why we observed a temporary (0–3 d) increase in pH above 4.0 before the pH drop commenced on approximately Day 4 (Fig. 4). The AMD mechanism resulting from the electrochemical dissolution of pyrite with and without CaF_2(aq) is shown in Fig. 5.

From Day 4 to 8, the pH in all of the pulp samples dramatically decreased. Over this period, Fe^{2+} ions were oxidized to Fe^{3+} ions, and the hydrolysis of Fe^{3+} increased the amount of H^+ ions. Meanwhile, as a strong oxidant, Fe^{3+} ions also promoted the oxidation of pyrite, thus further increasing H^+ ions in solution. Because F^- could stimulate pyrite electrochemical interactions resulting in increased H^+ ions in solution, the pyrite pulp

Table 4. Model parameters† for equivalent circuit of Fig. 3.

CaF_2	C_{dl}	R_t	CPE_p, Y_0	n	R_p
mg L^{-1}	F cm^{-2}	Ωcm²	S cm^{-2} s^{-n}		Ωcm²
0	1.010×10^{-3}	4.269×10^4	1.738×10^{-4}	0.8801	4.846×10^4
10	1.199×10^{-3}	4.025×10^4	1.796×10^{-4}	0.8797	4.825×10^4
50	1.310×10^{-3}	3.926×10^4	1.947×10^{-4}	0.8787	4.446×10^4
saturated	1.732×10^{-3}	3.247×10^4	2.088×10^{-4}	0.8740	3.515×10^4

† C_{dl}, double layer capacitance; R_t, charge transfer resistance; CPE_p, constant phase element; n, a dimensionless number revealing the degree of surface inhomogeneity; R_p, film resistance (Ozcan et al., 2008).

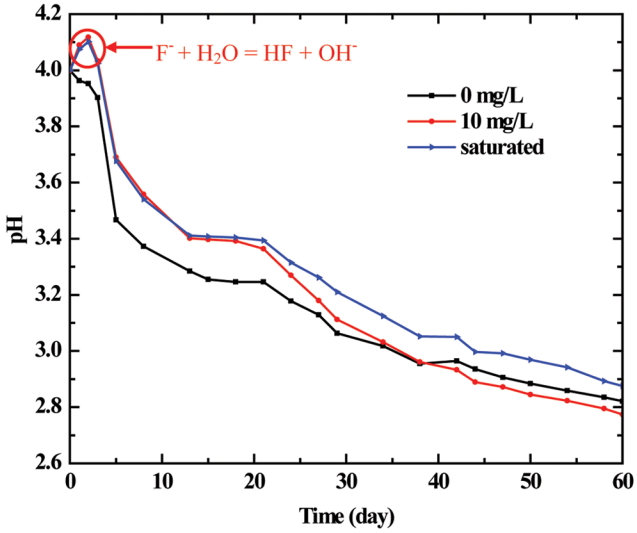

Fig. 4. The pH values of pyrite pulp in various concentrations of CaF_2 solutions.

pH decreased more dramatically with increases in the CaF_2(aq) concentration.

Between Day 8 and 20, the pyrite pulp pH decreased smoothly, that is, the pH curve flattened due to the occurrence of a cover layer (sulfur or iron-deficient sulfur-rich surface). The cover layer can effectively protect the pyrite surface from most ions and inhibit the electrochemical reaction. Therefore, the decrease in pH due to the promotion of the electrochemical dissolution of pyrite by F^- became less effective, and the increase in pH due to the hydrolysis reaction of F^- in solution became more effective, which increased the pulp pH as the CaF_2(aq) concentration increased during Days 12 to 20.

Between Day 21 and 60 of the reaction, the pyrite pulp pH decreased quickly. The intermediate cover layer transformed into sulfite or sulfate ions during this period stimulates pyrite electrochemical dissolution. The tendency of the pyrite pulp pH to decrease was due to the stimulation by the F^- ions promoting the electrochemical dissolution of pyrite. From Day 38 through 60, the pyrite pulp pH in the 10 mg L^{-1} concentration sample was lower than that without F^-.

Conclusions

Based on the established electrochemical parameters and the dynamic pH changes of pyrite in a sulfuric acid solution with different concentrations of CaF_2(aq), the following conclusions could be derived. (i) The polarization curve revealed that the presence of CaF_2(aq) prompted the electrochemical dissolution of pyrite. When the CaF_2(aq) concentration increased from 0 to 10 mg L^{-1} or was saturated, the corrosion current density of the pyrite electrode increased from 0.386 to 0.447 or 0.607 μA cm^{-2}, respectively. Their corresponding promoting efficiencies were 15.80 and 57.25%, respectively. This phenomenon results from the formation of FeF_2 from F^- and Fe^{2+}, while at a higher scan potential, F^- and Fe^{3+} form FeF_6^{3-} complex ions. (ii) Electrochemical impedance spectroscopy revealed the mechanism by which CaF_2(aq) stimulated the electrochemical dissolution of pyrite. First, the charge transfer resistance of the double layer decreased due to the formation of fluorinated iron complexes. Second, the passivation resistance of the cover layer decreased due to the strong penetration of F^- ions through it into the double layer. (iii) Initially, hydrolysis of F^- slightly increased the pH of the mine drainage. However, the AMD was dramatically affected by the electrochemical dissolution of pyrite due to CaF_2(aq). When pyrite is associated with high concentrations of CaF_2(aq), increased caution should be practiced and more attention should be focused on the environmental impacts. These current results are based on a laboratory study while the acidity of AMD may be affected by multiply factors in the field. Therefore, in the next step, field monitoring and investigating on the pyrite tailing associated with fluorite mineralization is of interest and concern. Practicable measures to inhibit the over acidification of pyrite mine drainage in the presents of CaF_2(aq) should be studied.

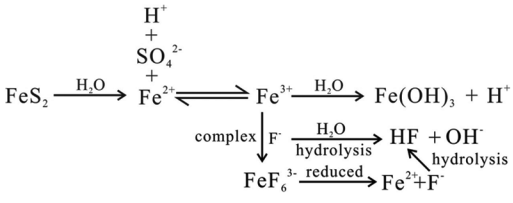

Fig. 5. The acid mine drainage mechanism of pyrite electrochemical dissolution with CaF_2 in the solution.

Acknowledgments

This work was financially supported by the 135 Program of the Institute of Geochemistry, CAS, the National Natural Science Foundation of China (40803017), the Key Technologies R & D Program of Guizhou Province, China (SY[2011]3088), and the 863 High Technology Research and Development Program of China (2010AA09Z207).

References

Alloway, B., and D.C. Ayres. 1997. Chemical principles of environmental pollution. 2nd ed. Blackie Academic & Professional, London.

Balci, N., W.C. Shanks, III, B. Mayer, and K.W. Mandernack. 2007. Oxygen and sulfur isotope systematics of sulfate produced by bacterial and abiotic oxidation of pyrite. Geochim. Cosmochim. Acta. 71:3796–3811. doi:10.1016/j.gca.2007.04.017

Bard, A.J., and L.R. Faulkner. 2001. Electrochemical methods: Fundamentals and applications. 2nd nd ed. Wiley & Sons, Hoboken, NJ.

Brindha, K., and L. Elango. 2011. Fluoride in groundwater: Causes, implications and mitigation measures In: S.D. Monroy, editor, Fluoride: Properties, applications and environmental management. Nova Press, New York. p. 111–136.

Bryson, L., and F. Crundwell. 2014. The anodic dissolution of pyrite (FeS_2) in hydrochloric acid solutions. Hydrometallurgy 143:42–53. doi:10.1016/j.hydromet.2014.01.005

Cabral, T., and I. Ignatiadis. 2001. Mechanistic study of the pyrite–solution interface during the oxidative bacterial dissolution of pyrite (FeS2) by using electrochemical techniques. Int. J. Miner. Process. 62:41–64. doi:10.1016/S0301-7516(00)00044-2

Chander, S., and A. Briceno. 1987. Kinetics of pyrite oxidation. Minerals and Metallurgical Processing 4:171–176.

Chandra, A.P., and A.R. Gerson. 2011. Pyrite (FeS_2) oxidation: A sub-micron synchrotron investigation of the initial steps. Geochim. Cosmochim. Acta 75:6239–6254. doi:10.1016/j.gca.2011.08.005

Chang, L.L.Y., R.A. Howie, and J. Zussman. 1998. Rock-forming minerals, Volume 5B, Non-silicates: Sulphates, carbonates, phosphates and halides. Geological Society, London.

Chen, G., J.M. Zen, F.R.F. Fan, and A.J. Bard. 1991. Electrochemical investigation of the energetics of irradiated FeS_2 (pyrite) particles. J. Phys. Chem. 95:3682–3687. doi:10.1021/j100162a045

Chernyshova, I. 2004. Pyrite oxidation mechanism in aqueous solutions: An in situ FTIR study. Russ. J. Electrochem. 40:69–77. doi:10.1023/B:RUEL.0000012077.98531.fe

Constantin, C., P. Chirita, and M. Preda. 2014. Characterization of pyrite reactivity by cyclic voltammetry. Revista de Chimie 65:215–218.

Constantin, C.A., and P. Chirita. 2013. Oxidative dissolution of pyrite in acidic media. J. Appl. Electrochem. 43:659–666. doi:10.1007/s10800-013-0557-y

España, J.S., E.L. Pamo, E. Santofimia, O. Aduvire, J. Reyes, and D. Barettino. 2005. Acid mine drainage in the Iberian Pyrite Belt (Odiel river watershed, Huelva, SW Spain): Geochemistry, mineralogy and environmental implications. Appl. Geochem. 20:1320–1356. doi:10.1016/j.apgeochem.2005.01.011

Evangelou, V., and Y. Zhang. 1995. A review: Pyrite oxidation mechanisms and acid mine drainage prevention. Environ. Sci. Technol. 25:141–199. doi:10.1080/10643389509388477

Galán, E., J. Gómez-Ariza, I. González, J. Fernández-Caliani, E. Morales, and I. Giráldez. 2003. Heavy metal partitioning in river sediments severely polluted by acid mine drainage in the Iberian Pyrite Belt. Appl. Geochem. 18:409–421. doi:10.1016/S0883-2927(02)00092-6

Gammons, C.H., T.E. Duaime, S.R. Parker, S.R. Poulson, and P. Kennelly. 2010. Geochemistry and stable isotope investigation of acid mine drainage associated with abandoned coal mines in central Montana, USA. Chem. Geol. 269:100–112. doi:10.1016/j.chemgeo.2009.05.026

Garand, A., and A. Mucci. 2004. The solubility of fluorite as a function of ionic strength and solution composition at 25°C and 1 atm total pressure. Mar. Chem. 91:27–35. doi:10.1016/j.marchem.2004.04.002

Geng, M., and Z. Duan. 2010. Prediction of oxygen solubility in pure water and brines up to high temperatures and pressures. Geochim. Cosmochim. Acta 74:5631–5640. doi:10.1016/j.gca.2010.06.034

Giannetti, B., C. Almeida, and S. Bonilla. 2006. Electrochemical kinetic study of surface layer growth on natural pyrite in acid medium. Colloids Surf. A Physicochem. Eng. Asp. 272:130–138. doi:10.1016/j.colsurfa.2005.07.018

Giannetti, B., S. Bonilla, C. Zinola, and T. Rabóczkay. 2001. A study of the main oxidation products of natural pyrite by voltammetric and photoelectrochemical responses. Hydrometallurgy 60:41–53. doi:10.1016/S0304-386X(00)00158-4

Greenwood, N.N., and A. Earnshaw. 1997. Chemistry of the elements. 2nd ed. Reed Educational and Professional Publishing Ltd, Woburn, MA.

Hall, S., J. Finch, and N. Rowlands. 1985. Enhancement of magnetic-susceptibility of pyrite by oxidative leaching. Transactions of the Institution of Mining and Metallurgy, Mineral processing and extractive Metallurgy. 96:C35–C39.

Hedin, R.S., R.W. Nairn, and R.L. Kleinmann. 1994. Passive treatment of coal mine drainage. US Bureau of Mines Information Circular 9389.35. US Department of the Interior, Washington DC.

Hiskey, J., and W. Schlitt. 1982. Interfacing technologies in solution mining. Proceedings of the Second SME-SPE International Solution Mining Symposium. Denver, CO. 18–20 Nov. 1981. AIME, New York.

Hocking, R.K., S.D. George, K.N. Raymond, K.O. Hodgson, B. Hedman, and E.I. Solomon. 2010. Fe L-Edge X-ray absorption spectroscopy determination of differential orbital covalency of siderophore model compounds: Electronic structure contributions to high stability constants. J. Am. Chem. Soc. 132:4006–4015. doi:10.1021/ja9090098

Ixer, R.A., B. Young, and C.J. Stanley. 1996. Bismuth-beating assemblages from the Northern Pennine Orefield. Mineral. Mag. 60:317–324. doi:10.1180/minmag.1996.060.399.06

Kelsall, G., Q. Yin, D. Vaughan, K. England, and N. Brandon. 1999. Electrochemical oxidation of pyrite (FeS_2) in aqueous electrolytes. J. Electroanal. Chem. 471:116–125. doi:10.1016/S0022-0728(99)00261-2

Lefebvre, M.C. 2002. Establishing the link between multistep electrochemical reaction mechanisms and experimental Tafel slopes. In: B.E. Conway, J.O'M. Bockris, and R.E. White. Modern aspects of electrochemistry Vol. 32. Springer, New York. p. 249–300. doi:10.1007/0-306-46916-2_3

Lehner, S., M. Ciobanu, K. Savage, and D.E. Cliffel. 2008. Electrochemical impedance spectroscopy of synthetic pyrite doped with As, Co, and Ni. J. Electrochem. Soc. 155:P61–P70. doi:10.1149/1.2885103

Lowson, R.T. 1982. Aqueous oxidation of pyrite by molecular-oxygen. Chem. Rev. 82:461–497. doi:10.1021/cr00051a001

Luther III, G.W. 1987. Pyrite oxidation and reduction: Molecular orbital theory considerations. Geochim. Cosmochim. Acta 51:3193–3199. doi:10.1016/0016-7037(87)90127-X

Macdonald, J.R. 1985. Generalizations of "universal dielectric response" and a general distribution-of- activation-energies model for dielectric and conducting systems. J. Appl. Phys. 58:1971–1978. doi:10.1063/1.336004

Marco, R.D., S. Bailey, Z.-T. Jiang, J. Morton, and R. Chester. 2006. An in situ chronoamperometry/synchrotron radiation grazing incidence X-ray diffraction study of the electrochemical oxidation of pyrite in chloride media. Electrochem. Commun. 8:1661–1664. doi:10.1016/j.elecom.2006.07.036

McKay, D.R. 1957. A kinetic study of the oxidation of pyrite in aqueous suspension. Retrospective Theses and Dissertations, 1919–2007. University of British Columbia, Vancouver.

Migaszewski, Z.M., A. Galuszka, S. Halas, S. Dolegowska, J. Dabek, and E. Starnawska. 2008. Geochemistry and stable sulfur and oxygen isotope ratios of the Podwisniowka pit pond water generated by acid mine drainage (Holy Cross Mountains, south-central Poland). Appl. Geochem. 23:3620–3634. doi:10.1016/j.apgeochem.2008.09.001

Moslemi, H., P. Shamsi, and F. Habashi. 2011. Pyrite and pyrrhotite open circuit potentials study: Effects on flotation. Miner. Eng. 24:1038–1045. doi:10.1016/j.mineng.2011.05.001

Mueller, B., F. Payer, D. Goswami, S. Kastury, J. Kornuc, C. Harman, et al. 2003. Technical and regulatory guidance document for constructed treatment wetlands. DTIC Document. Wetlands Team, US Interstate Technology and Regulatory Council, Washington DC.

Orazem, M.E., and B. Tribollet. 2008. Electrochemical impedance spectroscopy. 2nd ed. John Wiley & Sons, Hoboken, NJ.

Ouyang, Y., Y. Liu, R. Zhu, F. Ge, T. Xu, Z. Luo, and L. Liang. 2015. Pyrite oxidation inhibition by organosilane coatings for acid mine drainage control. Miner. Eng. 72:57–64. doi:10.1016/j.mineng.2014.12.020

Ozcan, M., F. Karadag, and I. Dehri. 2008. Investigation of adsorption characteristics of methionine at mild steel/sulfuric acid interface: An experimental and theoretical study. Colloids Surf. A Physicochem. Eng. Asp. 316:55–61. doi:10.1016/j.colsurfa.2007.08.023

Palencia, I., R. Wan, and J. Miller. 1991. The electrochemical behavior of a semiconducting natural pyrite in the presence of bacteria. Metall. Trans. B. 22:765–774. doi:10.1007/BF02651153

Pang, J., A. Briceno, and S. Chander. 1990. A study of pyrite/solution interface by impedance spectroscopy. J. Electrochem. Soc. 137:3447–3455. doi:10.1149/1.2086249

Peters, E., and H. Majima. 1968. Electrochemical reactions of pyrite in acid perchlorate solutions. Can. Metall. Q. 7:111–117. doi:10.1179/cmq.1968.7.3.111

Pratesi, G., and C. Cipriani. 2000. Selective depth analyses of the alteration products of bornite, chalcopyrite and pyrite performed by XPS, AES, RBS. Eur. J. Mineral. 12:397–409. doi:10.1127/ejm/12/2/0397

Ryzhenko, B.N. 1965. Determination of the dissolution constant of hydrofluoric acid and the conditions for replacement of calcite by fluorite. Geochem. Int. 2:196–199.

Sarmiento, A.M., V. Oliveira, J.L. Gomez-Ariza, J.M. Nieto, and D. Sanchez-Rodas. 2007. Diel cycles of arsenic speciation due to photooxidation in acid mine drainage from the Iberian Pyrite Belt (Sw Spain). Chemosphere 66:677–683. doi:10.1016/j.chemosphere.2006.07.084

Sheoran, A., and V. Sheoran. 2006. Heavy metal removal mechanism of acid mine drainage in wetlands: A critical review. Miner. Eng. 19:105–116. doi:10.1016/j.mineng.2005.08.006

Singer, P.C., and W. Stumm. 1970. Acidic mine drainage: The rate-determining step. Science 167:1121–1123. doi:10.1126/science.167.3921.1121

Solmaz, R., G. Kardaş, B. Yazıcı, and M. Erbil. 2008. Adsorption and corrosion inhibitive properties of 2-amino-5-mercapto-1, 3, 4-thiadiazole on mild steel in hydrochloric acid media. Colloids Surf. A Physicochem. Eng. Asp. 312:7–17. doi:10.1016/j.colsurfa.2007.06.035

Stern, M., and A.L. Geary. 1957. Electrochemical polarization. 1. A theoretical analysis of the shape of polarization curves. J. Electrochem. Soc. 104:56–63. doi:10.1149/1.2428496

Stumm, W., and G.F. Lee. 1961. Oxygenation of ferrous iron. Ind. Eng. Chem. 53:143–146. doi:10.1021/ie50614a030

Stumm, W., and J.J. Morgan. 1981. Aquatic chemistry: An introduction emphasizing chemical equilibria in natural waters. 2nd ed. John Wiley & Sons, New York.

Tachibana, M., K. Ishida, Y. Wada, M. Aizawa, and M. Fuse. 2009. Study of polarization curve measurement method for type 304 stainless steel in BWR high temperature-high purity water. J. Nucl. Sci. Technol. 46:132–141. doi:10.1080/18811248.2007.9711514

Taylor, B.E., M.C. Wheeler, and D.K. Nordstrom. 1984. Stable isotope geochemistry of acid mine drainage: Experimental oxidation of pyrite. Geochim. Cosmochim. Acta 48:2669–2678. doi:10.1016/0016-7037(84)90315-6

Veloso, T.C., L.C. Sicupira, I.C.B. Rodrigues, L.A.M. Silva, and V.A. Leao. 2012. The effects of fluoride and aluminum ions on ferrous-iron oxidation and copper sulfide bioleaching with Sulfobacillus thermosulfidooxidans. Biochem. Eng. J. 62:48–55. doi:10.1016/j.bej.2012.01.003

Wang, M., Y. Bai, W. Chen, B. Markert, C. Peng, and Z. Ouyang. 2012. A GIS technology based potential eco-risk assessment of metals in urban soils in Beijing, China. Environ. Pollut. 161:235–242. doi:10.1016/j.envpol.2011.09.030

Wang, X., H. Yang, and F. Wang. 2011. An investigation of benzimidazole derivative as corrosion inhibitor for mild steel in different concentration HCl solutions. Corros. Sci. 53:113–121. doi:10.1016/j.corsci.2010.09.029

Wang, Z., X. Xie, S. Xiao, and J. Liu. 2010. Comparative study of interaction between pyrite and cysteine by thermogravimetric and electrochemical techniques. Hydrometallurgy 101:88–92. doi:10.1016/j.hydromet.2009.11.015

Weber, P.A., W.A. Stewart, W.M. Skinner, C.G. Weisener, J.E. Thomas, and R.S.C. Smart. 2004. Geochemical effects of oxidation products and framboidal pyrite oxidation in acid mine drainage prediction techniques. Appl. Geochem. 19:1953–1974. doi:10.1016/j.apgeochem.2004.05.002

Yang, S.Q., and H.Y. Jiang. 1991. Electrochemical studies on pyrite. Acta Phys. Chim. Sin. 7:735–739.

Yeum, B. 2004. ZSimpWin Version 3.20. Electrochemical impedance spectroscopy data analysis software. EChem Software, Ann Arbor, MI.

Zhai, D.G., J.J. Liu, J.P. Wang, Y.Q. Yang, H.Y. Zhang, X.L. Wang, et al. 2014. Zircon U-Pb and molybdenite Re-Os geochronology, and whole-rock geochemistry of the Hashitu molybdenum deposit and host granitoids, Inner Mongolia, NE China. J. Asian Earth Sci. 79:144–160. doi:10.1016/j.jseaes.2013.09.008